Research Article Vol. 59, No. 5 / 10 February 2020 / Applied Optics 1253

applied optics

Optimization study of metallic sub-wavelength gratings as the polarizer in infrared wavelengths

Zongyao Yang,[1] Bo Feng,[1] Bingrui Lu,[1] Yifang Chen,[1,2,*] Wenhao Li,[3] Wei Zhang,[3] and Tao Li[4]

[1]Nanolithography and Application Research Group, State Key Lab of ASIC and System, School of Information Science and Engineering, Fudan University, Shanghai 200433, China
[2]Engineering Research Center of Advanced Lighting Technology, Fudan University, Shanghai, China
[3]Changchun Institute of Optics, Fine Mechanics and Physics, Chinese Academy of Science, China
[4]Key Laboratory of Infrared Imaging Materials and Detectors, Shanghai Institute of Technical Physics, Chinese Academy of Sciences, 500 Yu Tian Road, Shanghai 200083, China
*Corresponding author: yifangchen@fudan.edu.cn

Received 25 September 2019; revised 12 December 2019; accepted 20 December 2019; posted 20 December 2019 (Doc. ID 378636); published 4 February 2020

Despite the polarimetric detection in the infrared wavelengths of 8–10 μm being of great importance and broad applications, there has been limited addressing of the grating-based polarizers in this band. One of the main issues lies in the process incompatibility between the conventional nanofabrication technique and the II-VI materials such as HgCdTe, so that the direct integration of polarizers with sensors still remains a big challenge. This paper reports our recent work on optimizing the grating structures, materials, and nanofabrication processes for enhancing both the transmittance and the extinction ratio of polarizers on Si and/or ZnSe wafers, using numerical simulations for the grating design and electron beam lithography for the nanoscale pattern generation. By utilizing the finite-difference time-domain method, both the transmittance and the extinction ratio are maximized by optimizing the grating geometric dimensions and the duty cycle for two different grating materials of Al and Au for comparison. Based on the designed structures, nanofabrications of sub-wavelength gratings in both Al and Au are carried out, and the processes are compared for achieving high polarization performance. Optical characterizations of the fabricated polarizers demonstrate that both high transmittance and extinction ratio can be achieved in feasible parameters and the nano-process developed in this work.

https://doi.org/10.1364/AO.378636

1. INTRODUCTION

Sub-wavelength gratings in metals are characterized as promising polarizers for polarimetric detection in both visible and infrared wavelengths [1–6], being able to enhance the distinction of physical and chemical characteristics such as materials, roughness, and textures between the target and the background. Arising from the attractive characteristics of miniaturized dimensions, high integrity, large incident window, and high damage threshold, gratings-based polarizers are drawing growing efforts for applications in infrared polarization detectors [7]. Using the high-accuracy registration technique in electron beam lithography (EBL) [8], Au-gratings-based polarizers have been successfully integrated onto InP/InGaAs detectors [9] for detection in 1.0–1.6 μm. However, during the process, the baking temperature of the EBL resists must be kept below 90°C to avoid the instability of the bump-bonded indium pillars as the interconnection, significantly limiting processing freedom. Furthermore, the complicity of the optical property in InP/InGaAs confuses the local surface plasmonic modes in metallic gratings, causing an extinction ratio of only 18:1, which is over 50:1 once fabricated on a bare InP wafer. To avoid the incompatibility between the Si-based process and the III–V compounded detectors, gratings-based polarizers are fabricated on conventional substrates such as quartz wafers for visible wavelengths [10] and Si or ZnSe for infrared wavelengths. In this way, polarizers can be manufactured in high volume at low cost with limited restraints on the processing conditions. The drawback lies in the energy loss in coupling the polarizers to the detectors, which requires high performance of the polarization characteristics to compensate for the loss. Zhang *et al.* reported a process for Al grating polarizers on quartz for visible wavelengths based on lithographical patterning followed by plasma etch [10]. Although the extinction ratio of 75:1 has been achieved, the plasma etch to form the Al grating can induce damage to the substrate. On the other hand, despite the demands for polarimetric detections in 8–10 μm (e.g., laid and

flush-buried mine detection [11], plant growth monitoring in agriculture [12], and infrared photoconductive and photovoltaic detectors [13,14]), the polarizers in this region have been rarely addressed to the best of our knowledge.

In this work, an optimization study of the grating structure and the process for 8–10 μm polarizers have been conducted, aiming to achieve an overall insight into its optical performance governed by the grating materials as well as the geometric structures. Using the finite-difference time-domain (FDTD) method, systematic simulations are first carried out in designing the sub-wavelength gratings. Two different grating materials, such as Al and Au, and two different substrate materials, such as Si and ZnSe, respectively, are compared for achieving high transmittance with high extinction ratio. The effects of the grating profiles, the pitch and the height on the polarization, are then theoretically studied to maximize the optical performance. Guided by the simulation results, electron beam lithography is carried out with a lift-off process to form the metallic gratings. Optical characterizations prove the developed polarizer is of magnificent performance for applications in polarimetric detection.

2. DESIGN OF THE METALLIC GRATINGS

Figure 1 schematically illustrates the shape of the metallic gratings on the same substrate. In this work, Si and ZnSe, both of which are transparent in the infrared wavelengths, are used as the substrate. The design parameters are listed in Table 1, in which two different materials for the gratings, Al and Au, are compared. All the gratings have a rectangular shape of the cross section as schematically shown in Fig. 1(a). The aim of the theoretical study is to maximize both the transmittance and the extinction ratio of the metallic gratings in 8–10 μm by optimizing the parameters, based on solving the Maxwell equations using the FDTD simulation software supplied by Lumerical Ltd.

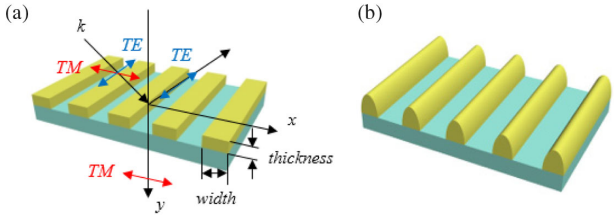

Fig. 1. Schematic for the metallic gratings being modeled in this work. Two different cross-sectional shapes of (a) rectangle and (b) parabola, two different materials for the gratings, aluminum (Al) and gold (Au), and two different substrate materials, Si and ZnSe, are compared, respectively.

Table 1. Simulated Parameters

Wave band	8–10 μm
Material	Al, Au
Substrate	Si, ZnSe
Thickness	100 nm
Period	400 nm
Duty cycle	0.5

In the FDTD simulation, the Palik model is applied for the metals of Au and Al; the periodic boundary condition is applied in the x direction, and the perfect matching layer condition is in the y direction [15]. The grating pitch is important to ensure the sufficiently high extinction ratio. However, if it is too short, the success yield in nanofabrication of gratings will drop rapidly. Under the sub-wavelength condition with the ease in nanofabricaiton, the pitch of 400 nm was adopted in this work.

Figure 2 presents the simulated transmittance [Fig. 2(a)] and the extinction ratio [Fig. 2(b)] of the gratings in both Al and Au. No matter whether Al or Au is used as the grating material, the gratings on the ZnSe give rise to much higher transmittance than those on Si. The main reason is that ZnSe has much higher transmittance than Si in the wavelength region of interest [Fig. 2(c)], and the thickness of both substrate materials is 500 μm. Therefore, ZnSe is selected as the polarizer substrate.

With ZnSe as the substrate, the kinds of the metals have great impacts on the extinction ratio. Figure 2(b) shows that the Al grating has much higher extinction ratio than Au grating under the assumption that the grating profile is rectangle. However, the fabricated Al gratings have a parabolic profile, as illustrated in Fig. 1(b), instead of rectangular one, so the extinction ratio is considerably reduced [16]. On the other hand, the cross-section profiles of the fabricated Au gratings are often relatively closer to the rectangular shape [9], resulting in an extinction ratio comparable to that of the Al grating with a rectangular shape. Therefore, in the selection of Al or Au as the grating material, the real structural shapes, as discussed above, need to be considered in the performance optimization.

Numerical simulations for Al gratings with rectangular and parabolic profiles, respectively, are carried out and presented in Figs. 2(d) and 2(e). The comparisons between the results show that the transmittances through the Al gratings with the rectangular and the parabolic shapes are not quite distinct, as both values are beyond 70%. However, the extinction ratio of the Al gratings with a rectangular cross section is much higher than that with a parabolic shape.

Furthermore, the polarization characteristics governed by the grating geometric structure are also studied by the FDTD method, which is applied for the Au gratings on the ZnSe substrate. Figure 3 presents both the transmittance and the extinction ratio in the 2D width-thickness planes of the grating with the pitch fixed to be 400 nm, with the grating-width changing from 160 to 240 nm (duty cycle 0.4–0.6) and the grating-thickness from 50 to 150 nm. Figures 3(a)–3(b) are for the wavelength of 8 μm and Figs. 3(c)–3(d) for 10 μm. Such 3D curves provide us with a clear overview of both the transmittance and the extinction ratio controlled by the grating geometric dimensions. The optimized zones satisfying the requirements for both the transmittance ($\geq$70%) and the extinction ratio ($\geq$50 : 1) can be easily figured out in the width-thickness planes as shown in Fig. 3. These zones guide us in adopting the optimized grating width and grating thickness. Based on the feasibility of the nano-process, the duty cycle of 0.5 and the grating thickness of 100 nm are well in the optimized areas, and these are adopted in the nanofabrication of sub-wavelength gratings in this work.

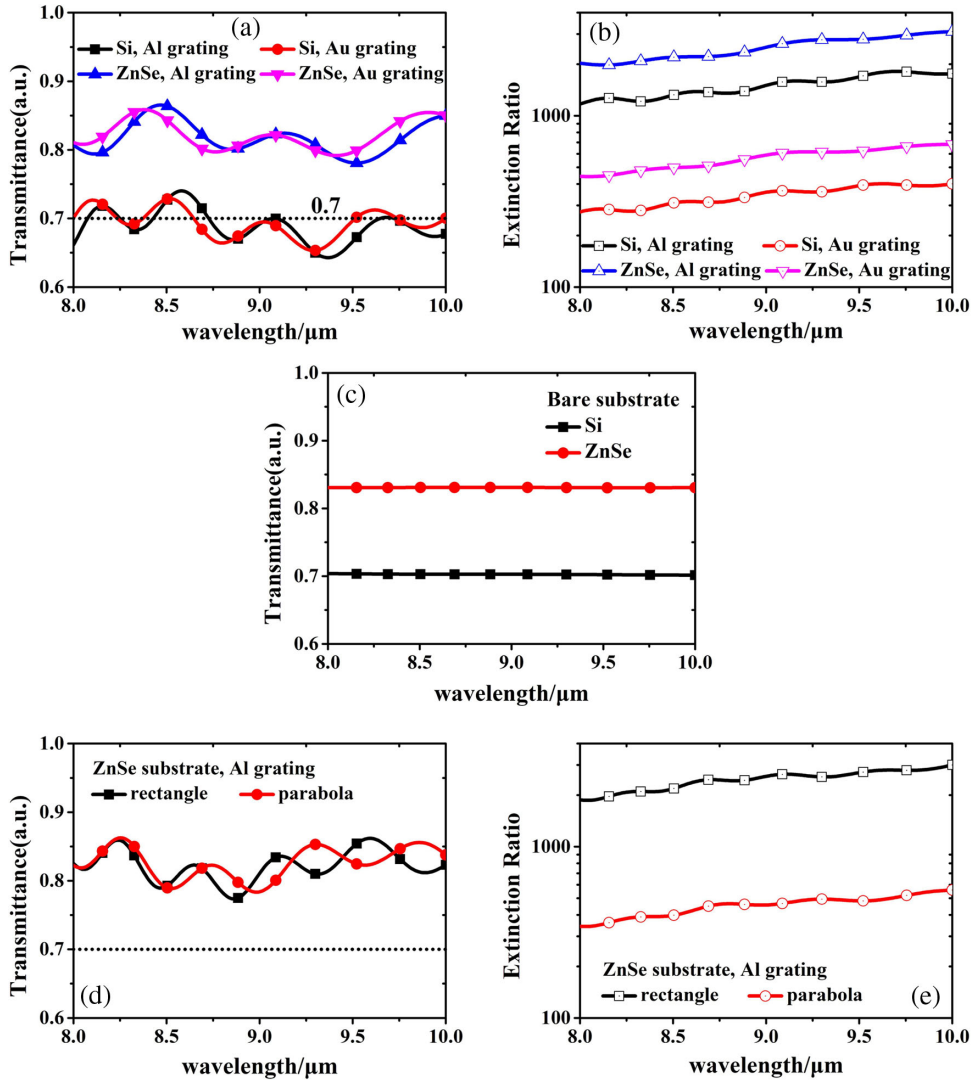

Fig. 2. Theoretical comparisons of the (a) transmittance and (b) extinction ratio of Al and Au gratings on Si and ZnSe substrates, respectively. (c) Comparison of the transmission through the bare substrates of Si and ZnSe. Comparisons of the (d) TM transmittance and (e) extinction ratio of Al gratings with rectangular and parabolic shapes on the ZnSe substrate.

3. OPTIMIZATION OF THE NANO-PROCESS

Since both Si and ZnSe are transparent in the infrared wavelengths in 1–14 μm, the sub-wavelength gratings as polarizers are fabricated on the two substrates for comparison.

A. Al and Au Gratings on Si Substrate

In this work, a bilayer of 380 nm PMMA-MAA (EL 11)/170 nm PMMA (MW950K) was applied to fabricate the Al gratings on Si. As comparison, a single layer of 450 nm PMMA (MW350K) was also spin-coated to fabricate the Au gratings. To ensure full glass transition of the resists, all the coated resists were baked in an oven for 1 h at 180°C. E-beam exposure was carried out by a state-of-the-art beamwriter, JEOL JBX6300, with a beam of 10 nm at 100 keV as the acceleration tension. After exposure, the resist was developed in the mixture of methyl isobutyl ketone (MIBK) and isopropanol (IPA) (1:3) for 60 s at 23°C and thoroughly rinsed in IPA for 30 s. Careful dose tests for optimizing the best profiles in the resists were conducted before the polarizers were fabricated. Both the 100 nm Al and Au were deposited by the thermal evaporation. The unwanted metals were finally removed by stripping off the resists in the lift-off process in acetone. Figures 4(a)–4(b) present the fabricated gratings in Al and Au on silicon with the nominal thickness of 100 nm. The Al grating lines are more like a parabolic shape, while the Au grating ones are more square-like, which is in accordance with paper [16], showing that the shape fabricated by the lift-off process after the thermal evaporation is parabolic, caused by the trench closure.

B. Au Gratings on ZnSe Substrate

Again, the state-of-the-art EBL was carried out on a single layer of 450 nm PMMA (MW350K) spin-coated on a ZnSe wafer, which was baked in an oven for 1 h at 180°C. To avoid the charging effect, a 60 nm conducting e-spacer layer, supplied by Allresist Ltd., was spin-coated on the top of the PMMA

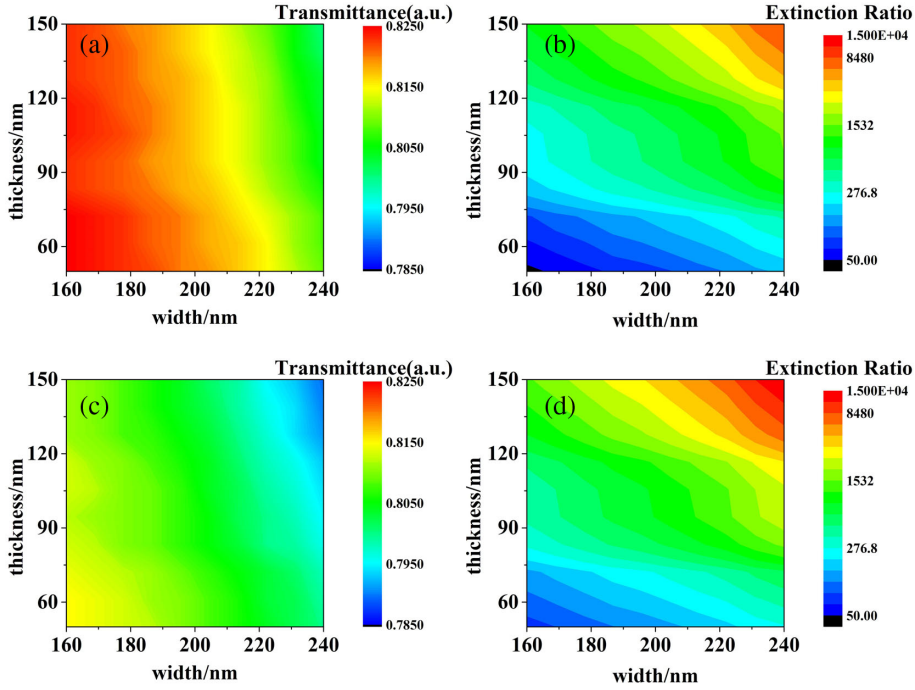

Fig. 3. Simulated transmittances of the TM component in the grating line width-thickness plane at (a) $\lambda = 8$ μm and (c) $\lambda = 10$ μm, respectively. The simulated extinction ratios in the width-thickness plane at (b) $\lambda = 8$ μm and (d) $\lambda = 10$ μm, respectively. In all the simulations, the cross-section shape of the grating is assumed to be rectangular.

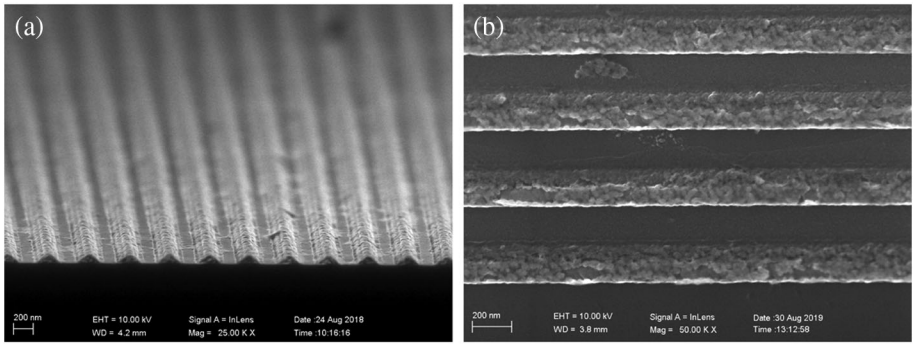

Fig. 4. Micrographs by scanning electron microscope (SEM) for the fabricated Al gratings in the sectional view (a) with 250 nm line width and Au gratings in the tilt angle of 45° and (b) with 200 nm line width on Si substrates.

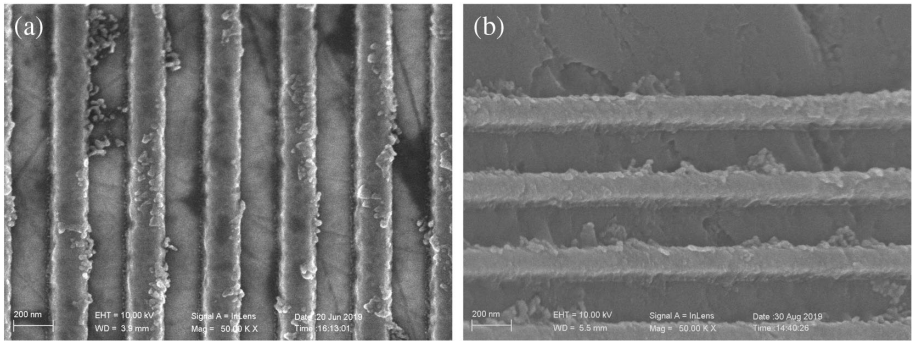

Fig. 5. Micrographs by SEM for the fabricated Au gratings with 200 nm line width with (a) the top view and (b) the tilt angle of 45° on the ZnSe substrate. The line cross-sectional shape looks more like a rectangle.

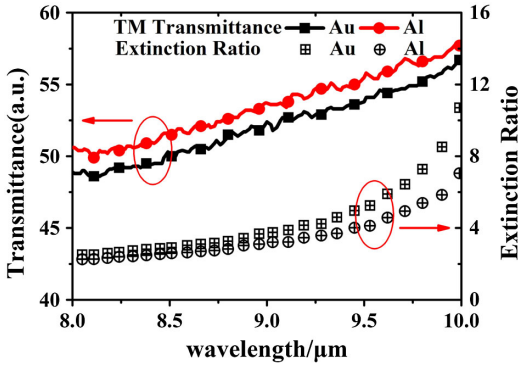

Fig. 6. Measured polarization properties of Au and Al gratings on Si.

and baked on a hot plate at 90°C for 2 min. After the e-beam exposure as described above, the e-spacer was first removed by rinsing in deionized water for 2 min before the routine developing process. It was found in our work that the adoption of an e-spacer was definitely necessary despite the weak conduction of the ZnSe substrate. Figure 5 shows the fabricated Au gratings on ZnSe with the nominal thickness of 100 nm. The fabricated sub-wavelength gratings were then subjected to the optical characterizations for further study of their polarimetric behaviors.

4. OPTICAL CHARACTERIZATIONS

A. Comparison of the Polarization Characteristics Between Al and Au Gratings on Si

Optical characterization was carried out in standard thermo infrared spectrum testing equipment in the long infrared wavelength band (8–10 μm). As shown in Fig. 6, the transmittance of Al gratings is higher than that of Au gratings, but the extinction ratio is the opposite, which is contrary to the simulation results as given above. This is because the cross-section structure of the fabricated Al gratings is parabolic, as shown in Fig. 4(a), while the simulated results were based on the model with the rectangular shape of the Al lines. This explains the distinction between the simulated and the measured results. However, the measured extinction ratios of the sub-wavelength gratings with both Al and Au metals are generally much smaller than the numerically simulated ones as presented in Fig. 2(b). This is because the structural difference between the real grating and the modelled one in the simulation can cause significant reduction of the ratio. Clear defects in the fabricated gratings can be seen in Fig. 5, which should be responsible for the major loss of the ratio in practice. Nevertheless, it is clear that the parabolic shape of the sub-wavelength grating enhances the transmittance and the rectangular one is beneficial to the extinction ratio [16]. To ensure high transmittance as well as high extinction ratio, Au gratings should be more favorable than Al in developing gratings-based polarizers, considering that the cross-sectional shape of the fabricated Au gratings is more square-like.

Furthermore, the measurement results also indicate that the extinction ratios of the gratings for both Al and Au are not satisfactorily high when Si is used as the substrate. ZnSe substrate, with higher transmittance than Si, should be employed.

B. Polarization Performance of the Au Gratings on ZnSe

Optical characterizations were then carried out on the fabricated Au gratings on the ZnSe substrate. Figure 7 shows the measured transmittances and extinction ratios for the gratings with line widths of 180 nm [Fig. 7(a)] and 200 nm [Fig. 7(b)], respectively. It can be seen that the extinction ratios are significantly

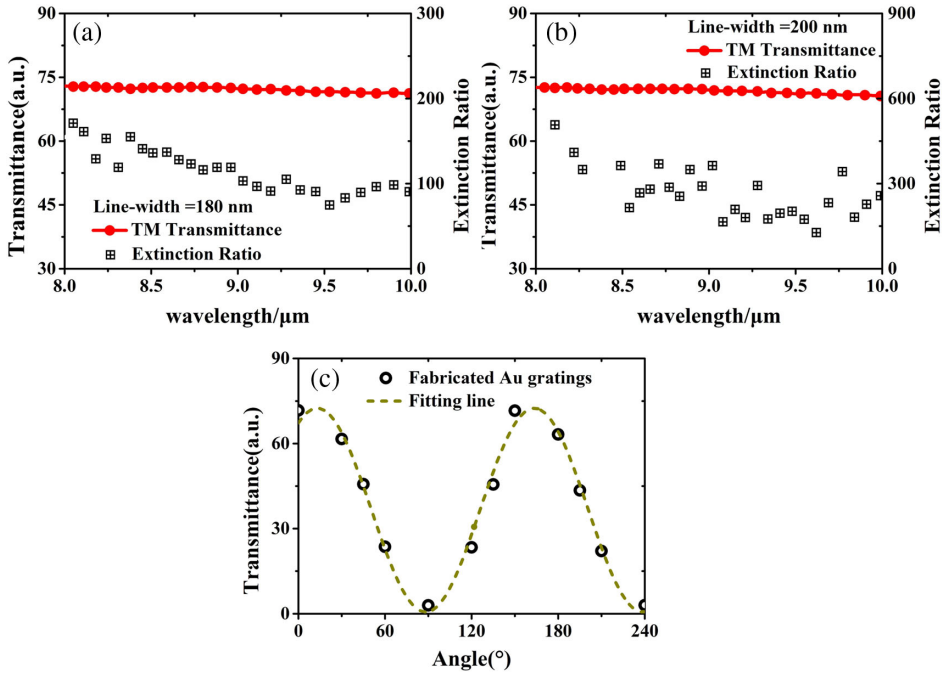

Fig. 7. Optically measured polarization properties of Au gratings with (a) 180 nm and (b) 200 nm line widths. (c) Polarization behavior of the transmitted light for the linear incident light at 9 μm. The open dots are the measured data, and the dashed line is the fitting line for eye guidance only.

enhanced by 1 order of the magnitude for the line width increasing from 180 up to 200 nm in correspondence to the duty cycle being increased from 0.45 to 0.5, while the transmittances are also as high as over 70%. Therefore, the duty cycle should be another important factor in optimizing the extinction ratio. It reaches its maximum when the duty cycle is fixed at 0.5. Such a significant polarization performance also originates from the ZnSe substrate being used as well as the rectangler shape of the Au lines as shown by the scanning electron microscope (SEM) photo in Fig. 5(b).

Figure 7(c) shows the polarization property of the fabricated Au grating with 180 nm width by measuring the transmittance (the open dots) changing with the azimuth angle of the incident light through the gratings at 9 μm. The dashed line is the fitting curve as a guide to the eye. The maximum polarization transmittance of our gratings is 72.3%, and the minimum is 0.69%, giving rise to the extinction ratio of 105:1, which can be further enhanced by using either the grating width of 200 nm (duty cycle 0.5) or 150 nm thickness.

5. CONCLUSIONS

The optimization study of the grating materials, the grating geometric parameters, and the substrate materials for sub-wavelength metallic gratings-based polarizers has been systematically carried out using the FDTD method in this work. The optimum grating parameters, such as the width and the thickness with a fixed pitch, have been determined for maximized polarimetric performance. Although Al gratings demonstrate higher transmittance and higher extinction ratio than when Au is used from the simulated results, the parabolic shape of the grating after nanofabrication deteriorates the polarimetric performance. Instead, Au is finally adopted for the polarizers on ZnSe, which gives rise to satisfactory performance as far as both the transmittance and the extinction ratio concerned. The optimization method proposed in this work should be generally applicable for other light bands for the development of commercial gratings-based polarizers as a whole.

Funding. Fudan University CIOMP Joint Fund (FC2017-008); Open Project of SITP (IIMDKFJJ-18-09); National Natural Science Foundation of China (61574043, U1732104); Zhejiang Lab's International Talent Fund for Young Professionals; Shanghai Technology Innovation Center (STCSM2019-11-20).

Acknowledgment. This work is financially supported by the following projects: the Fudan University CIOMP Joint Fund, the Open project of SITP, National Natural Science Foundation of China, the Zhejiang Lab's International Talent Fund for Young Professionals.

Disclosures. The authors declare that there are no conflicts of interest related to this paper.

REFERENCES

1. G. P. Nordin, J. T. Meier, P. C. Deguzman, and M. W. Jones, "Micropolarizer array for infrared imaging polarimetry," J. Opt. Soc. Am. A **16**, 1168–1174 (1999).
2. J. Liang, L. Ren, E. Qu, B. Hu, and Y. Wang, "Method for enhancing visibility of hazy images based on polarimetric imaging," Photon. Res. **2**, 38–44 (2014).
3. J. Guo and D. Brady, "Fabrication of thin-film micropolarizer arrays for visible imaging polarimetry," Appl. Opt. **39**, 1486–1492 (2000).
4. K. M. Twietmeyer, R. A. Chipman, A. E. Elsner, Y. Zhao, and D. Vannasdale, "Mueller matrix retinal imager with optimized polarization conditions," Opt. Express **16**, 21339–21354 (2008).
5. S. Gao, R. Njuguna, and V. Gruev, "Fabrication and performance evaluation of pixelated nano-wire grid polarizer," Proc. SPIE **8873**, 88730L (2013).
6. V. Gruev, "Fabrication of a dual-layer aluminum nanowires polarization filter array," Opt. Express **19**, 24361–24369 (2011).
7. D. Sun, T. Li, B. Yang, X. M. Shao, X. Li, and Y. F. Chen, "Research on polarization performance of InGaAs focal plane array integrated with superpixel-structured subwavelength grating," Opt. Express **27**, 9447–9458 (2019).
8. Y. F. Chen, "Nanofabrication by electron beam lithography and its applications: a review," Microelectron. Eng. **135**, 57–72 (2015).
9. R. Wang, T. Li, X. M. Shao, X. Li, X. Q. Huang, J. H. Shao, Y. F. Chen, and H. M. Gong, "Subwavelength gold grating as polarizers integrated with InP-based InGaAs sensors," ACS Appl. Mater. Interfaces **7**, 14471–14476 (2015).
10. Z. G. Zhang, F. L. Dong, T. Cheng, K. Qiu, Q. C. Zhang, W. G. Chu, and X. P. Wu, "Nano-fabricated pixelated micropolarizer array for visible imaging polarimetry," Rev. Sci. Instrum. **85**, 105002 (2014).
11. M. Larive, D. Spoliansky, and O. Trezieres, "Preprocessing of 8- to 12-um polarimetric features for laid and flush-buried mine detection," Proc. SPIE **3710**, 197–202 (1999).
12. Q. Huang, Q. Zhou, and L. Zhang, "An overview of crop growing condition monitoring in China agriculture remote sensing monitoring system," Proc. SPIE **7384**, 73840N (2009).
13. E. P. G. Smith, L. T. Pham, G. M. Venzor, E. M. Norton, M. D. Newton, P. M. Goetz, V. K. Randall, A. M. Gallagher, G. K. Pierce, E. A. Patten, R. A. Coussa, K. Kosai, W. A. Radford, L. M. Giegerich, J. M. Edwards, S. M. Johnson, S. T. Baur, J. A. Roth, B. Nosho, T. J. De Lyon, J. E. Jensen, and R. E. Longshore, "Hgcdte focal plane arrays for dual-color mid- and long-wavelength infrared detection," J. Electron. Mater. **33**, 509–516 (2004).
14. J. M. Dell, J. Antoszewski, M. H. Rais, C. Musca, J. K. White, B. D. Nener, and L. Faraone, "HgCdTe mid-wavelength IR photovoltaic detectors fabricated using plasma induced junction technology," J. Electron. Mater. **29**, 841–848 (2000).
15. A. Taflove and S. C. Hagness, *Computational Electrodynamics: the Finite-Difference Time-Domain Method*, 3rd ed. (Artech House, 2005).
16. C. Xu, J. N. Deng, X. Q. Huang, T. Li, X. Li, X. M. Shao, R. Wang, H. M. Gong, S. C. Zhang, J. H. Shao, and Y. F. Chen, "Integrating subwavelength polarizers onto InP-$In_xGa_{1-x}As$ sensors for polarimetric detection at short infrared wavelength," Photon. Nanostruct. Fundam. Appl. **33**, 10–15 (2019).